Structural Engineering and Mechanics, Vol. 20, No. 5 (2005) 589-608
DOI: http://dx.doi.org/10.12989/sem.2005.20.5.589

Tensile response of steel/CFRP adhesive bonds for the rehabilitation of civil structures

F. Matta†

Department of Structural & Transportation Engineering, University of Padua, Via Marzolo, 9, 35131, Padua, Italy

Vistasp M. Karbhari‡

Department of Structural Engineering, MC-0085, University of California San Diego, La Jolla, CA 92093-0085, USA

Renato Vitaliani‡†

Department of Structural & Transportation Engineering, University of Padua, Via Marzolo, 9, 35131, Padua, Italy

(Received August 26, 2004, Accepted April 19, 2005)

Abstract. There is a growing need for the development and implementation of new methods for the rapid and cost-effective rehabilitation of deteriorating steel structural components to offset the drawbacks related to welding and/or bolting in the field. Carbon fiber reinforced polymer (CFRP) composites provide a potential alternative as externally bonded patches for strengthening and repair of metallic structural members for building and bridge systems. This paper describes results of an investigation of tensile and fatigue response of steel/CFRP joints simulating scenarios of strengthening and crack-patching. It is shown that appropriately designed schemes, even when fabricated with levels of inaccuracy as could be expected in the field, can provide significant strain relief and load transfer capability. A simplified elasto-plastic closed form solution for stress analysis is presented, and validated experimentally. It is shown that the bond development length remains constant in the linear range, whereas it increases as the adhesive is deformed plastically. Fatigue resistance is shown to be at least comparable with the requirements for welded cover plates without attendant decreases in stiffness and strength.

Key words: steel; carbon fiber reinforced polymer composite; rehabilitation; bond; tensile strength; fatigue.

---

† Graduate Student, Now at Center for Infrastructure Engineering Studies, University of Missouri-Rolla, Rolla, MO 65409-0710, USA
‡ Professor, Corresponding author, E-mail: vkarbhari@ucsd.edu
‡†Professor

1. Introduction

Worldwide there are a significant number of ageing metallic structural components and systems, such as in cast iron and steel framed industrial building and structures, tunnel linings, and bridges, which are showing increasing signs of deterioration and reduced functionality. Over a quarter of the bridges in the 2002 US National Bridge Inventory are classified as either structurally deficient or functionally obsolete with about half of these involving steel superstructure (National Bridege Inventory 2002). Of these systems, steel stringer and truss bridges present the greatest potential for rehabilitation (Dunker *et al.* 1987). Problems of similar magnitudes are being experienced in Europe (Hollaway and Cadei 2002) and Japan (Nishikawa *et al.* 1998). The substantial increase in traffic on existing life-lines, including bridges, puts a high premium on keeping these facilities open and in service. However, increases in required load levels and in overall levels of traffic can lead to excessive deflection, increased fatigue related deterioration, and decreased functionality. Often, these systems require strengthening in order to ensure that they both meet load requirements and contemporary design and safety specifications. Lack of routine inspection and inadequate maintenance in addition to the effect of the harsh and changing environment exacerbate the deterioration of the built infrastructure. In the case of metallic structural components corrosion is a major instrument of degradation with effects accruing from the use of deicing salt on roads potentially producing a more severe effect on bridges than due to a marine environment (Albrecht and Hall 2003).

Beyond these factors, aspects such as detailing can also have a strong effect. In the presence of fatigue sensitive details, such as fillet welds, the cyclic action of live loads can result in unexpected cracking, with risks of catastrophic failure (Fisher 1984). The continuity inherent in welded structures makes it possible for a crack to propagate from an element into an adjoining one, and failure can occur at nominal stress levels substantially lower than that associated with failure as assumed in the initial design. In such cases, repair is desirable to restore the original load capacity, unless the gravity of the damage calls for the replacement of weakened components, or of the complete structure.

Conventional techniques of repair and strengthening involve welding, riveting or bolting of additional material. While these techniques are effective they suffer from some noticeable disadvantages – they often add additional weight to an already weakened system; they can be costly and time consuming; they often require the introduction of fatigue sensitive details, and the additional components often result in accelerated corrosion. In addition, the modifications often result in the introduction of stress concentrations and thermal locked-in stresses which further weaken the system, albeit in a different manner from the initial deficiency. There is thus a need for the development and implementation of new methods of conducting cost-effective, rapid and functionally effective repairs and strengthening.

Although the efficacy of adhesively bonded composite plates, or patches, as a means of strengthening and arresting cracks has been demonstrated and implemented successfully in the marine (Grabovac 2003) and aerospace (Baker and Jones 1988, Poole 2002) sectors, for the most part these applications relate to thin skins or local cracks. The use in civil infrastructure, to date, has been limited. Some research has demonstrated the intrinsic efficiency and convenience of steel to steel adhesive bonding in the repair of metallic structural components (Albrecht and Sahli 1988, Nara *et al.* 1985). The potential benefit of repairing distressed steel girders with FRP composites was demonstrated over a decade ago by Sen and Liby (1994). However, due to the relatively lower modulus of the FRP patch, and the thermoelastic mismatch it was noted that the effect was substantially constrained, and that clamps/bolts were needed to prevent detachment especially close to, and subsequent to, local yielding of steel. In a series of papers Karbhari and Shulley (1995), Shulley *et al.* (1994), McKnight *et al.* (1994), Bourban *et al.* (1994) investigated the durability of bonds between FRP composites and structural steel with emphasis on repair of corroded areas in the web of "I" girders. A structural investigation on scale beams using these results was undertaken by Shulley (1994). Tavakkolidazeh and Saadatmanesh reported that the fatigue life of steel beams with fatigue cracks at the tension flange could be significantly extended via bonded repairs (Tavakkolidazeh and Saadatmanesh 2003a). Epoxy bonding of carbon fiber reinforced composite sheets was also examined as a possible option to strengthen slab-on-girder bridge members (Tavakkolidazeh and Saadatmanesh 2003b) with patch ends tapered to reduce peel stresses. Although the method was rapid and effective it did not allow for increases in structural stiffness. In a companion study the use of composite patches was investigated as a means of rehabilitation of simulated local section loss in the tension flange and it was reported that strength and stiffness could be recovered as long as brittle failure due to peel-induced debonding was avoided (Tavakkolidazeh and Saadatmanesh 2003c). Fatigue tests to assess the effectiveness of strengthening riveted steel bridge members damaged by fatigue were conducted by Colombi *et al.* (2003) and it was noted that on small scale specimens, fatigue life of center notched steel plates could be increased by factors of 3-16. A full scale fatigue test on a 91-year old girder was successfully completed by Bassetti *et al.* (2000), and scale tests were conducted by Jones and Civjan (2003) who reported that as a result of crack patching fatigue life could be extended by up to 54% for samples with center holes and 115% for those with edge notches. The criticality of integrity of adhesive bonds was emphasized in the study. A comprehensive program aimed at the use of carbon fiber reinforced polymer (CFRP) composites to strengthen old and deteriorating cast-iron and steel components has been undertaken by Moy *et al.* (2000), Moy (2002), as a result of which a number of flexural and compression members along the London Underground have been rehabilitated. In addition, a set of preliminary guidelines for composite based strengthening of metallic structures has been developed (FRP Composites: Life Extension and Strengthening of Metallic Structures 2001).

Although a number of studies have been conducted at the level of beams, there is a lack of data at the fundamental level related to the efficiency of patching, and the comparison between predicted and experimental results at the level of adhesive bond, which is critical for the development of a comprehensive design approach. For further implementation of such techniques in the field, under varying climatic conditions and on metallic substrates that have undergone varying amounts of deterioration and section loss, a thorough understanding of the variables and of bond configurations through experimental and analytical means is essential. This paper reports on the aspects of characterization of the ability of bonds to transfer loads corresponding to critical levels such as the yield point of steel, and to validate an analytical model capable of being used for design. It also assesses the ability of the rehabilitation schemes to meet fatigue threshold requirements prescribed by Eurocode 3 (1992) and the AASHTO LRFD Bridge Design Specifications (1998) for details commonly present in rehabilitated steel bridge members.

2. Materials and test setup

In order to simulate conditions replicate of structural sections, A36 hot rolled steel bars were used.

Based on tests conducted on the bars the yield strength, ultimate strength, and Young's modulus were determined to be 305.7 MPa, 445.2 MPa and 196 GPa, respectively, with standard deviations of 7.9 MPa, 7.7 MPa and 4.8 GPa, respectively. Prefabricated composite strips are commonly used in the rehabilitation of concrete, and have been shown to have uniform and reliable performance. Since the focus of this paper is on the use of readily available material forms, rather than of materials development, type S Carbodur® strips with an average thickness of 1.33 mm were used. The strips were determined to have average strengths, longitudinal modulus and Poisson's ratio of 2,990 MPa, 165.7 GPa and 0.3, respectively with standard deviations of 340 MPa, 5.8 GPa and 0.02, respectively. The ultimate strain was an average of 1.79%, which is higher than the manufacturer provided value of 1.7%. A two component high-strength filled epoxy adhesive, Sikadur 30® was selected. The adhesive has a pot life of about 70 minutes at 23°C and an average glass transition temperature as measured using dynamic mechanical thermal analysis (DMTA) of 96.4°C. The average shear strength (at 14 day cure) was determined to be 24.8 MPa, whereas the average tensile strength and modulus were determined to be 24.8 MPa and 4.5 GPa, respectively. The Poisson's ratio has a typical value of 0.35.

Test specimens were configured in the form of doubler joints with the composite strips bonded on either side of the steel section as shown in Fig. 1. The first set of specimens, representative of cases where rehabilitation is required to enhance strength and stiffness such as along the flange of a flexural section, consisted of intact steel coupons of 24.8 mm width and 7.9 mm thickness sandwiched between composite plates of 410 mm lengths centered over the steel coupon. The total splice length exceeds that recommended by Hart-Smith (2002) and thus enables the splice to not only withstand creep and load rate effects, but to also provide a level of fatigue disband tolerance. The specimens are denoted as skin doubler specimens (SDS). In a number of cases, there is need to rehabilitate the section to allow load redistribution and to prevent local buckling (if in the form of a

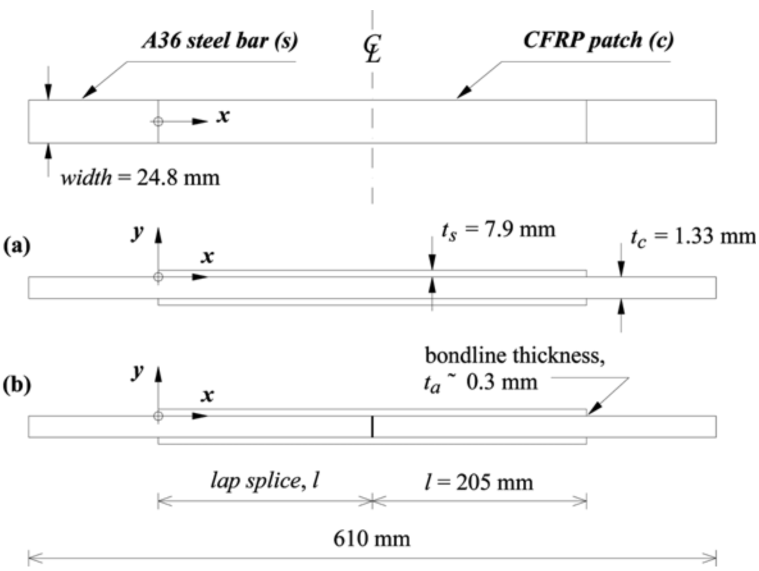

Fig. 1 Schematic of test specimens showing dimensions (not to scale) (a) skin doubler specimen (SDS), (b) double strap specimen (DSS)

"H" of "I" section) and premature failure, such as when corrosion causes loss of steel section, or when a section is cracked. In order to simulate this case, two steel coupons were butted end-to-end at the center, representing an extreme case of through section cracking, and the composites were bonded on either side. These specimens were denoted as double strap specimens (DSS). From a rehabilitation perspective, it should be noted that in the first case the goal would be to attain the expected strain relief within the base specimen material with bond failure occurring significantly after yielding of steel, whereas in the second it would be to increase fatigue life and enable stiffness and load capacity to be regained, or, if appropriate (as in the case of under-strength sections), to be increased. Prior to bonding, the steel specimens were thoroughly degreased and then sandblasted and cleaned to remove residue. It should be noted that since the rehabilitation would ultimately be conducted in the field rather than in controlled laboratory settings, the procedures used for surface preparation were not designed to be precise, but rather were representative of current fabrication procedures. While this can result in a degree of variation between specimens, it ensures that results are representative of those that could reasonably be expected in the field during rehabilitation of actual structural components. Similarly, although it is advantageous to complete the bonding immediately after surface preparation, to avoid formation of an oxide layer, the specimens were allowed to remain in ambient conditions for 3 days to simulate logistical conditions likely to be faced in the field on bridges. The composite strips were cleaned using methylethylketone (MEK) and then adhesively bonded onto the steel, with application of C-clamps for pressure during ambient curing of the adhesive. Pressure application was only through hand tightening of C-clamps again keeping in mind the logistics of field rehabilitation. The resulting bond line was fairly uniform with an average thickness of 0.3 mm. Prior to testing the excess adhesive was removed by sanding and each specimen was instrumented extensively with strain gauges. With reference to Figs. 1, 5 gauges were placed on the SDS specimens at distances of 7, 23, 37, 205 and 397 mm from the end of the joint (shown as the origin in Figs. 1(a)), and 6 gauges were placed on the DSS specimens at distances of 105, 162, 182, 202, 242 and 305 mm from the end of the joint (shown as the origin in Fig. 1(b)). Additional gauges were placed on some specimens in areas of interest such as close to ends.

Monotonic tensile tests were conducted using a servo-hydraulic test machine at a constant loading rate of 0.5 kN/s till failure by separation of adherends was attained. Load, displacement and strain

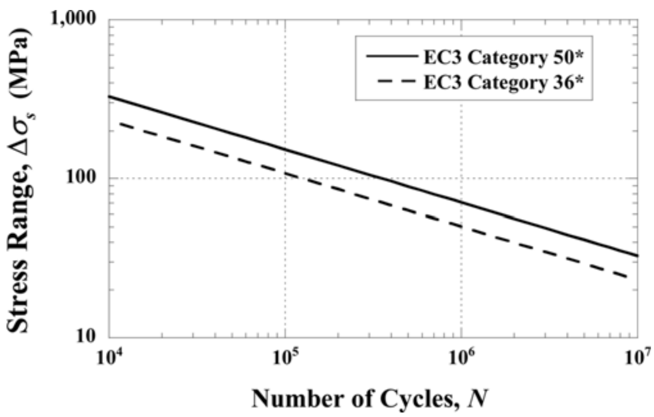

Fig. 2 Fatigue thresholds for EC category 36* and 50* categories (Stress ranges refer to unbonded steel sections)

were measured continuously. Fatigue tests were also conducted on both sets of specimen types to assess capabilities in accordance with the fatigue thresholds for EC3 categories 36* and 50* (European Committee for Standardization 1992) (as shown in Fig. 2) and AASHTO category E and E' details, as required for splice plates welded onto tension members for purposes of rehabilitation (American Association of State Highway and Transportation Officials 1998).

3. Load transfer analysis

In order to provide an assessment of response a simple one-dimensional analytical model was developed using the following assumptions: (a) materials comprising the adherends and adhesives are linear elastic; (b) composite adherends have fibers oriented in the loading direction; (c) the adhesive shear stress-strain constitutive response is elastic-perfectly plastic with perfect bonding; (d) shear stress, τ_a, in the adhesive layer is constant through the bond-line thickness, t_a; (e) the axial stress at the inner and outer adherend, σ_i and σ_o, respectively are constant through the thicknesses t_i and t_o, respectively; and (f) secondary bending due to eccentricity can be neglected. Using the specimen configuration and coordinate system in Fig. 1 the elastic closed form solution for the adhesive shear stress as initially expressed by Albat and Romilly (1999) can be stated as

$$\tau_a(x) = \tau_{a,x=0}[e^{-\lambda x} - e^{-\lambda(2l-x)}] \qquad 0 \le x \le 2l\ (2l = 410\ \text{mm}) \tag{1}$$

for the SDS configuration, and

$$\tau_a(x) = \tau_{a,x=0}e^{-\lambda x} + \tau_{a,x=l}e^{-\lambda(l-x)} \qquad 0 \le x \le l\ (l = 205\ \text{mm}) \tag{2}$$

for the DSS configuration (which is anti-symmetric in $l \le x \le 2l$. The stress distribution parameter, λ, is given as

$$\lambda = \sqrt{\frac{G_a}{t_a}\left(\frac{1}{E_s t_s} + \frac{1}{E_c t_c}\right)} \tag{3}$$

where G_a is the adhesive shear modulus, E_s and E_c are the elastic moduli of the steel and composite, respectively, and t_a, t_s, and t_c are the thicknesses of the adhesive, steel and composite, respectively. The expressions in (1) and (2) can essentially be thought of as sums of the distribution function

$$\tau_a(x) = \tau_{a,\max}e^{-\lambda x} \tag{4}$$

at each critical load transfer zone, which is in line with a model commonly accepted in design practice (Baker and Jones 1988). Since the shear stresses are assumed to be constant across the thickness of the adhesive layer, the peaks in the stress, $\tau_{a,\max}$, are located at discontinuities where $x = 0$ in the appropriate coordinate systems shown in Fig. 1, instead of at a small distance from the ends. However, for purposes of the current analysis this simplification causes insignificant errors. Since the adherends are not wide enough to neglect effects of Poisson's ratio, plain strain conditions ($\varepsilon_z = 0$) are assumed. From (4) if k is taken to be less than 1 and represents the ratio between the load transferred over a distance L and the load transfer capacity at the critical zone under consideration, L can be determined as

$$L = \frac{\ln[(1-k)^{-1}]}{\lambda} \tag{5}$$

and remains constant as long as the adhesive is deformed elastically. If a load transfer efficiency of 95% of theoretical is attained, $k = 0.95$, the effective transfer length can be expressed as

$$L = L_{eff} = \frac{4}{\lambda} \tag{6}$$

For a given applied load per unit width, P, $\tau_{a,\max}$ can be determined through consideration of simple equilibrium conditions as

$$\tau_{a,\max} = \frac{\lambda PS}{[2(1+S)]} \le \tau_p \tag{7}$$

at the ends of the composite patches, and

$$\tau_{a,\max} = \frac{\lambda P}{[2(1+S)]} \le \tau_p \tag{8}$$

at the central cut section, i.e., at $x = l$ for the DSS configuration, where S is the stiffness ratio

$$S = \frac{E_c t_c}{E_s t_s} \tag{9}$$

and τ_p is the linear limit of the adhesive shear stress when assuming an elastic-perfectly plastic constitutive model as suggested by Hart-Smith (2002). Therefore, load transfer is confined within an effective length at the section discontinuities, with a virtually zero-stress trough in between, which signifies the limit to bond strength developable for a given joint configuration (Hart-Smith 2002).

Considering the specimen materials and dimensions used in this investigation, $\lambda = 0.1803$, $S = 0.287$ and $\tau_p = 24.8$ MPa. Therefore, the tensile loads, F_e, beyond which plastic transition of the bonds occurs can be theoretically calculated as 30.5 kN for the SDS configuration ($P_e = 1,234$ N/mm), and 8.8 kN for the DSS configuration ($P_e = 354$ N/mm). The latter is the minimum value obtained from (7) and (8), which yield the same result in case of stiffness balanced joints, thus indicating the maximum structural efficiency for the double strap configuration. The corresponding theoretical adhesive shear stress peak at the composite patch ends is 24.8 MPa and 7.1 MPa for the SDS and DSS configurations, respectively. In this case, due to the imbalance in the adherends stiffness, the stress distribution along the DSS overlap is rendered non-symmetric, and reaches the maximum value of 24.8 MPa at $x = l$, where the less stiff adherend extends.

The theoretical strain distribution, in the composite, $\varepsilon_c(x)$, in the domain $0 \le x \le l$ (it is symmetric in $l \le x \le 2l$), at a given P, can be readily found by integration of (1) and (2) with respect to x, and the dividing by $E_c t_c$, as

$$\varepsilon_c(x) = \frac{1}{E_c t_c}\int_0^x \tau_{a,x=0} e^{-\lambda x} dx = \tau_{a,x=0}\frac{1-e^{-\lambda x}}{\lambda E_c t_c} \tag{10}$$

for the SDS configuration where $\tau_{a,x=0}$ is calculated using (7), and

$$\varepsilon_c(x) = \frac{1}{E_c t_c}\int_0^x [\tau_{a,x=0} e^{-\lambda x} + \tau_{a,x=l} e^{-\lambda(l-x)}] dx = \tau_{a,x=0}\frac{1-e^{-\lambda x}}{\lambda E_c t_c} + \tau_{a,x=l}\frac{e^{-\lambda l}(e^{\lambda x}-l)}{\lambda E_c t_c} \tag{11}$$

for the DSS configuration, where $\tau_{a,x=0}$ and $\tau_{a,x=l}$ are calculated using (7) and (8) respectively.

It should be noted that although linear elastic approaches may be effective in dealing with relatively brittle adhesives, even limited ductility can result in plastic shear stress response plateaus which are sufficiently long to affect $L_{eff.}$ The length of the plateau, L_p, to be added to (5) to determine the total anchorage length at each load transfer zone, can be estimated as

$$L_p = \frac{(T_c - \tau_p/\lambda)}{\tau_p} = \frac{T_c}{\tau_p} - \lambda^{-1} > 0 \tag{12}$$

where T_c is the total load per unit width transferred at the point of section discontinuity and τ_p/λ is the corresponding value of maximum load transfer per unit width in the elastic range. Since the adhesive shear stress is constant over L_p, $\varepsilon_c(x)$ varies linearly in the bond interval.

The local simplified solutions for adhesive shear stress, load transfer and effective length at the patch end zones and at the central cut, are then expressed as

$$\tau_{a(x)} = \tau_{a,\max} e^{-\lambda x} \tag{13}$$

$$T_c(x) = \frac{\tau_{a,\max}(1 - e^{-\lambda x})}{\lambda} \tag{14}$$

$$L_{eff} = \frac{n}{\lambda} \tag{15}$$

where n represents a measure of effective length defined as $\ln[(1-k)^{-1}]$. For linear elastic behavior ($L_p = 0$), where $\tau_{a,\max}$ is calculated through (7) at the patch ends and (8) at the mid section butt joint, and n is based on (5) with

$$L_{eff} = \frac{n}{\lambda} + L_p \tag{16}$$

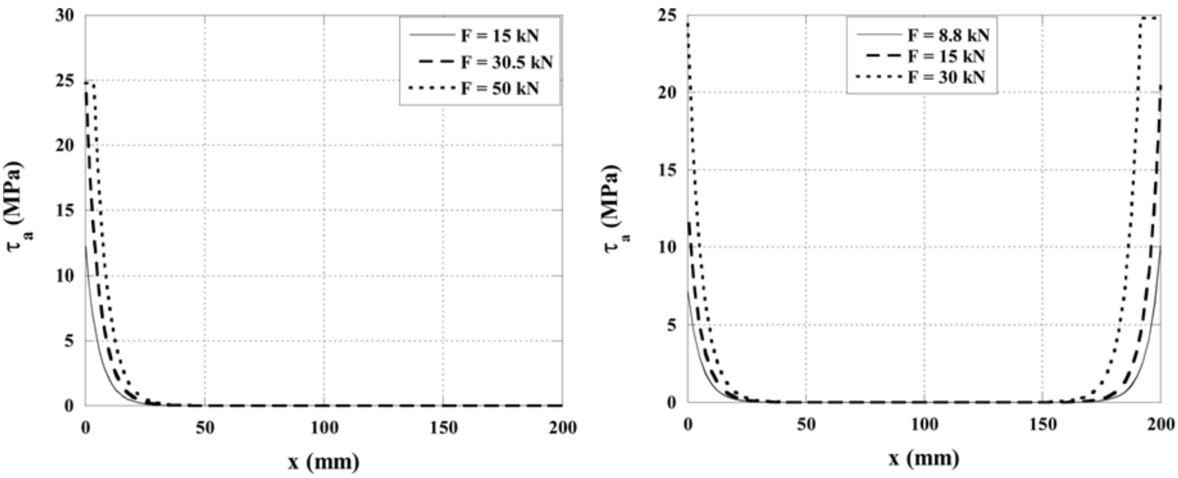

(a) (b)

Fig. 3 Theoretical adhesive shear stress distribution in the $0 \le x \le l$ domain (a) SDS configuration ($F = 30.5$ kN represents load beyond which plastic transition occurs), (b) DSS configuration ($F = 8.8$ kN represents load beyond which adhesive plastic transition occurs) and

$$\tau_a(x) = \begin{cases} \tau_p & (x \le L_p) \\ \tau_p e^{-\lambda(x - L_p)} & (x > L_p) \end{cases} \tag{17}$$

$$T_c(x) = \begin{cases} \tau_p x & (x \le L_p) \\ \tau_p\left[L_p + \dfrac{e^{-\lambda(x - L_p)}}{\lambda}\right] & (x > L_p) \end{cases} \tag{18}$$

Using the above outlined analytical procedure, examples of theoretical distributions of the adhesive shear stress at different load levels for the SDS and DSS configurations over $0 \le x \le l$ are shown in Fig. 3. It can be see that the effect of stiffness imbalance in the DSS configuration with plastic deformation in the adhesive at the central butt joint occurs at relatively low loads, and that τ_a at the ends of the composite patch is well below the maximum limit of $\tau_p = 24.8$ MPa.

4. Results and discussion

4.1 Response to monotonic tensile loading

The overall response characteristics of the SDS and DSS configurations, in comparison to the unbonded steel, are shown in Fig. 4 and Table 1. As can be seen in Fig. 4 there is very little variation between specimens within the same set, although both the bonded configurations show a bit more statistical variation than the virgin steel specimens. It can also be seen that all bonded specimens (SDS and DSS) showed a significant increase in stiffness over the virgin steel specimens. In the case of the SDS configuration failure was initiated at both patch ends at an average strain level of about 1173 $\mu\varepsilon$, as measured from strain gauges located on the composite close to both ends. A comparison of typical strain development as a function of load and position of strain gauges on

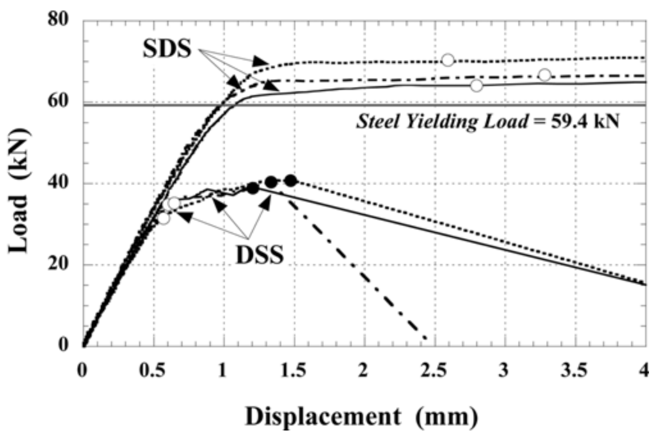

Fig. 4 Comparison of SDS and DSS response under monotonic tension loading (Unfilled and filled circles indicate locations of initiation of disband initiation and patch separation, respectively)

Table 1 Overall response characteristics of steel-CFRP adhesive bonded joint specimens

Specimen type	Disbond initiation		Failure		$\varepsilon_{c,SG4}$	$\frac{\varepsilon_{c,SG4}}{\varepsilon_{cu}}$	$\frac{\varepsilon_{c,SG4}}{\varepsilon_{sy}}$
	Load (kN)	Stress (MPa)	Load (kN)	Stress (MPa)	($\mu\varepsilon$)	(ε_{cu} = 17900 $\mu\varepsilon$)	(ε_{sy} = 1560 $\mu\varepsilon$)
SDS (unfatigued)	66.9	343	68	349	1330	0.07	0.85
SDS (fatigued)	66.9	344	69	352	1401	0.08	0.90
DSS (unfatigued)	34.2	175	40	206	3603	0.20	2.31
DSS (fatigued)	32.8	168	34	176	3129	0.17	2.01

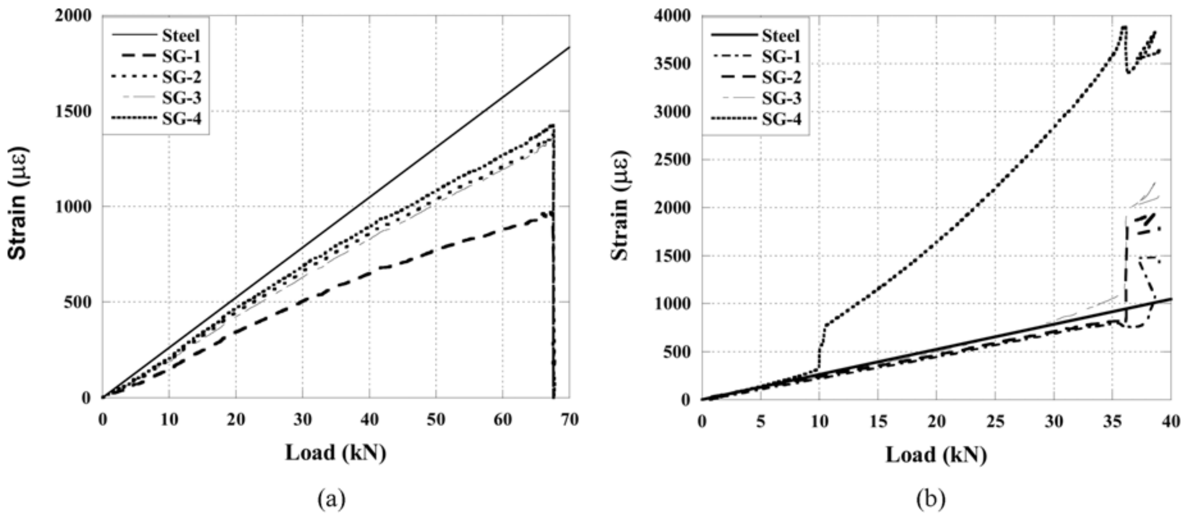

Fig. 5 Typical strain development as a function of load (a) SDS configuration. SG-1, SG-2, SG-3 and SG-4 represent positions of strain gages placed at 7 mm, 23 mm, 37 mm and 205 mm (midpoint of composite strip) from the end of the CFRP composite patch, (b) DSS configuration. SG-1, SG-2, SG-3 and SG-4 represent positions of strain gages placed at 105 mm, 168 mm, 182 mm and 205 mm (midpoint of composite strip, above the butt joint) from the end of the CFRP composite patch

the FRP composite and on a virgin steel bar is shown in Fig. 5(a). The CFRP patch is noted to provide a strain relief of about 20%, with the subsequent stiffening effects. Debond initiation is observed after attainment of the elastic limit of steel, which occurred at an average load of 59.4 kN, emphasizing the effectiveness of the composite to delay yield. As can be seen, there is a fairly constant level of strain attained among gauges from 23 mm away, especially at lower load levels, showing this to be close to the critical transfer length, which is calculated as 22.2 mm for loads less than the elastic limit, and as 28.4 mm for F = 65 kN. Disbonding was in all cases adhesive over the entire length, initiating at ends apparently due to out-of-plane peeling effects (Fig. 6(a)). It should be noted that since bonding was conducted 3 days after sandblasting, a residual oxide film was clearly visible on the steel surfaces. Although this is undesirable, it is likely to occur in a civil construction environment. However, failure took place at loads greater than twice that associated with plastic transition of the joints, under tension, underlining the overall effectiveness of the strengthening scheme even under this situation. Following (Karbhari and Shulley 1995) the

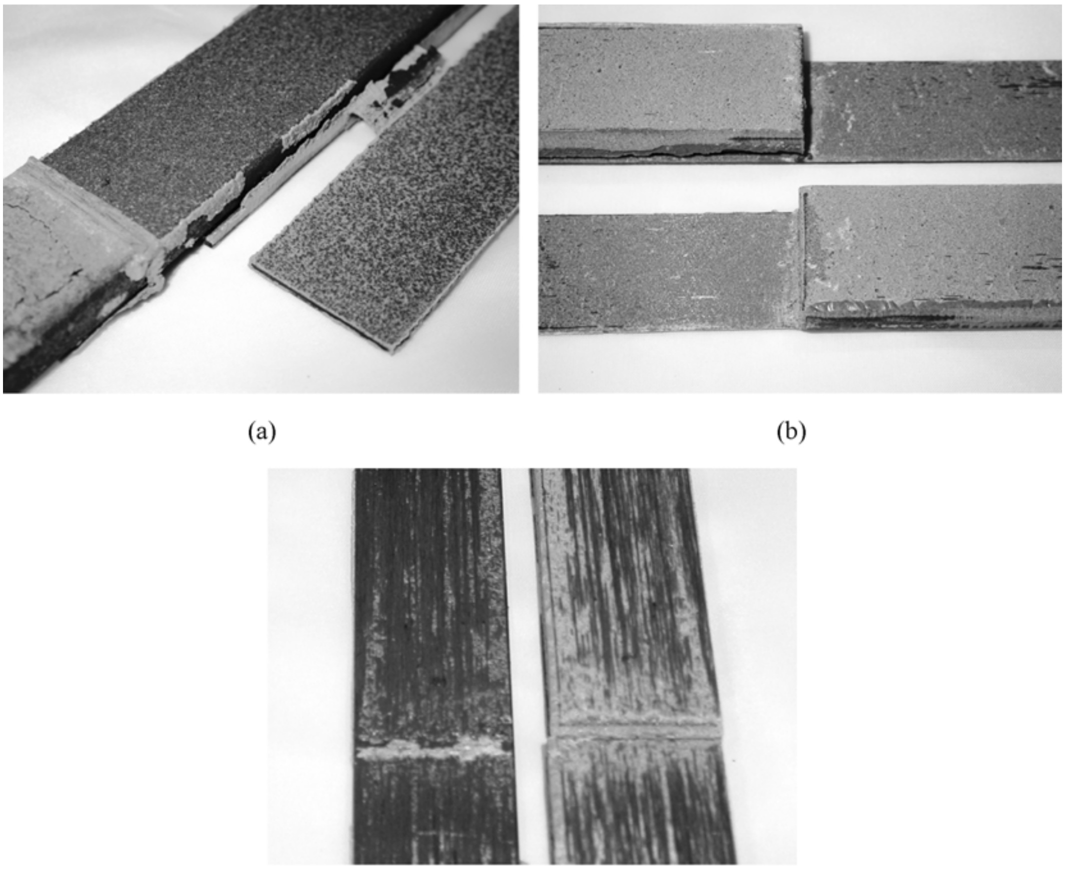

(a) (b)

(c)

Fig. 6 Typical fracture initiation surfaces (a) adhesive at steel/epoxy interface in a SDS specimen, (b) cohesive fracture initiation surfaces in the adhesive in a monotonically loaded DSS specimen, (c) fiber-matrix level debonding within the CFRP composite patch in a fatigued DSS specimen

magnitude of peel stresses at the linear elastic limit is

$$\sigma_{y,\max} = \tau_p \left[\frac{3E_a'(1-\nu_c^2)t_c}{E_c t_a} \right]^{1/4} \tag{19}$$

which in the current case can be computed as 21.2 MPa wherein the Young's modulus of the adhesive is corrected to consider the constraining effect of adherends, i.e., $E_a' = 7266$ MPa, pursuant to the formulation by Wang and Rose (1997). Considering the actual configuration details stress values of about 24.8 MPa were likely achieved in the adhesive prior to interfacial failure. Thus, although the failure mode itself was unsatisfactory the SDS configuration showed good performance with about a 22% level of strain relief.

A comparison of strain development in the DSS configuration is shown in Fig. 5(b). An early, sharp increase in ε_c as measured over the butt-joint region (SG-4 in Fig. 4(b)) identifies the rupture of the adhesive joint between the ends of the steel adherends as the initiator of cracking and subsequent debonding. It is noted that strains measured at other locations mirror those measured on

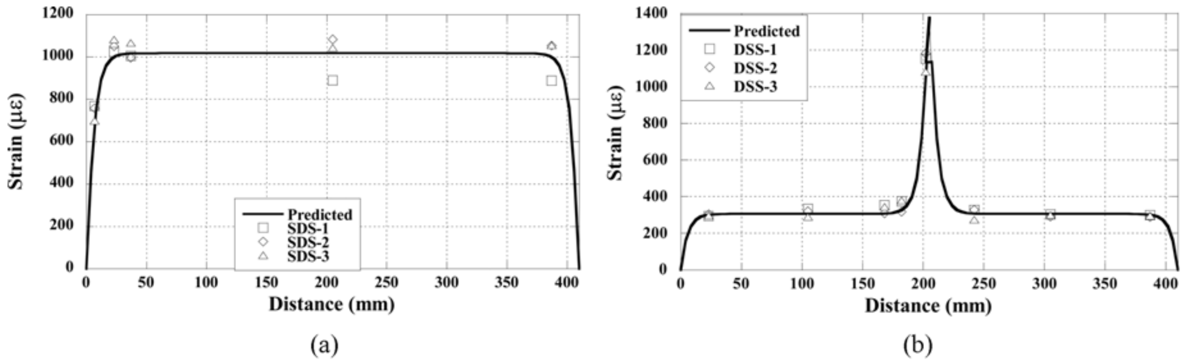

Fig. 7 Comparison between predicted and experimental strains (a) SDS configuration at F = 50 kN, (b) DSS configuration at F = 12 kN

a virgin steel bar, indicating that away from the butt-joint the development of strain is not affected by the break in the steel represented by the joint.

The crack initiating from the butt-joint eventually resulted in debonding and separation along the composite-steel bond-line. From Table 1 it can be noted that, once the crack initiated, the average strain measured at location SG-4 was about 3603 $_{\mu}\varepsilon$, which is on average 0.20 times the value of $\varepsilon_{c,u}$ and 2.31 times the value of $\varepsilon_{s,y}$ (=1,560 $_{\mu}\varepsilon$). Besides the quality of the fabrication procedure, two major factors can be expected to affect the failure mode of the DSS configuration: (a) the peel stresses acting at the ends of the composite strip, which tend to detach the composite from the steel adherend similar to that seen in the SDS configuration, and (b) the shear stress peak combined with relatively small normal stresses, which were compressive and thus anti-peel. Consequently, failure due to opening at the patch ends (mode I) or sliding at the mid-section (mode II), rather than breakage of the adherends, is expected. Because of the elastic stiffness mismatch between the adherends, the maximum shear stress at x = 205 mm was far greater than that at the bonded patch ends for a given load level (Fig. 3(b)). Hence, peeling effects were less critical than shear stresses at the central cut, where failure initiated cohesively in the epoxy based adhesive (Fig. 6(b)). Disbonds generally proceeded in a mixed mode in cohesive/interlaminar fashion. When interfacial steel/adhesive debond occurred it was confined to within a few centimeters of the ends of the composite strip which is indicative of peel-induced separation as observed in the skin doubler specimens. The occurrence of edge effects was suggested by the presence of local arch-shaped interlaminar disbond surfaces in the composite.

A comparison of analytical predictions of $\varepsilon_c(x)$ using Eqs. (10) and (11) with actual measurements al load levels beyond the initial plastic transition are shown in Fig. 7 and indicate good agreement. It is seen that the agreement is similar at other load levels with the percentage error generally being between 3-6% and not greater than 12%. It is also noted that the theoretically derived values of P (using Eqs. (7) and (8)) are consistent with those applied experimentally and observed in the SDS and DSS configurations.

4.2 Response to tensile fatigue loading

Fatigue tests were run on a set of SDS and DSS configuration samples for 1 million cycles. For the SDS configuration fatigue cycling was conducted at a stress range, $\Delta\sigma_s$, of 83 MPa (corresponding to minimum and maximum load levels of 0.85 kN and 17 kN, respectively) and a stress ratio, R, of 0.05 at a frequency of 10 hz. It should be noted that following (7) the limiting tensile load for linear elastic response ($F_{e,SDS} = Pw$) can be expressed as

$$F_{e,SDS} = \frac{2\tau_p(1+S)w}{\lambda S} = 30.5 \text{ kN} \tag{20}$$

where w is the specimen width (w = 24.8 mm in this case) τ_p is the linear limit for the adhesive shear stress given by the shear strength $\tau_{a,u}$ = 24.8 MPa under assumptions of elastic-perfectly plastic response (Hart-Smith 1973) and S = 0.2875. Also the stress distribution parameter, λ, described earlier in (3) has a value of 0.1804. Since the value of $F_{e,SDS}$ = 30.5 kN corresponds to an axial stress of 157 MPa on an unbonded steel bar, the adhesive shear stress associated with the fatigue range can be expected to be well below the elastic limit. Intermittent overload was simulated by subjecting the specimens to a 0-50-0 kN load-unload block every 250,000 cycles (at N = 0 cycles, 250000 cycles, 500000 cycles, 750000 cycles, and 1000000 cycles) at a 0.5 kN/s rate. Changes in the structural response were assessed by recording the applied load and crosshead displacement during these blocks, and after every 10,000 cycles. The maximum load, which is greater than 70% of the ultimate load, induces a corresponding axial stress of 257 MPa in the gross steel section outside the joint, i.e., 84% of the yield stress. Fig. 8 depicts the adhesive shear stress at the CFRP laminate end zones based on classical beam-spring theory (Hart-Smith 1973), where load transfer takes place, at F = 0.85, 17 and 50 kN, and the fatigue shear and peel stress ranges. A comparison of the fatigue load levels with the typical response of a skin doubler specimen (SDS) tested in tension is depicted in Fig. 9. It is noted that the steel yielding load is 59.4 kN.

During its service life, a rehabilitated section will not be normally subjected to the stress range assumed. However, since in most cases, strengthening is implemented on metallic sections reduced

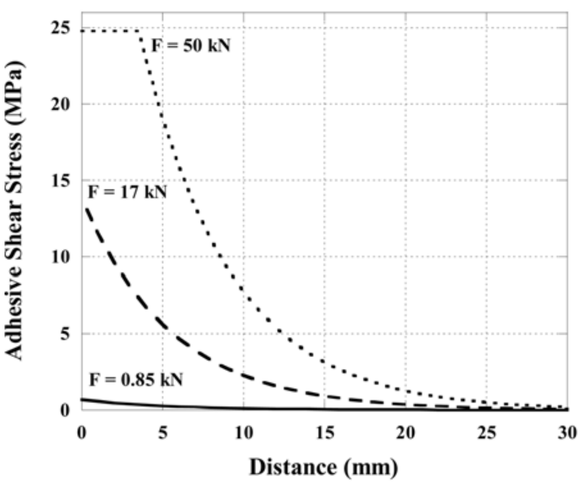

(a)

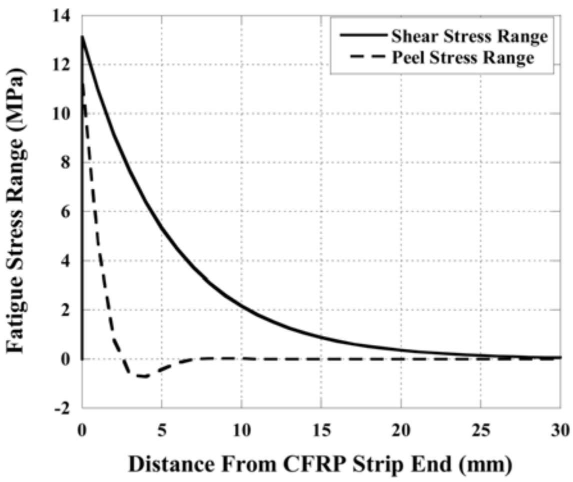

(b)

Fig. 8 Theoretical shear stress development in the CFRP patch end zones for the SDS configuration (a) at minimum (0.85 kN), maximum (17 kN) and intermittent overload (50 kN) fatigue load levels, (b) shear and peel stress ranges in fatigue

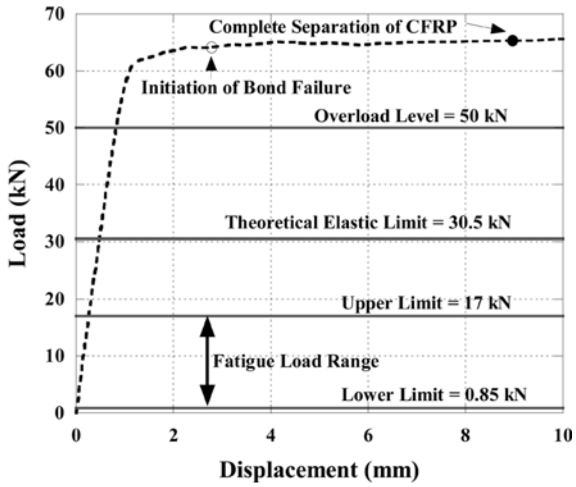

Fig. 9 Fatigue load levels in comparison to a typical SDS configuration response in tension

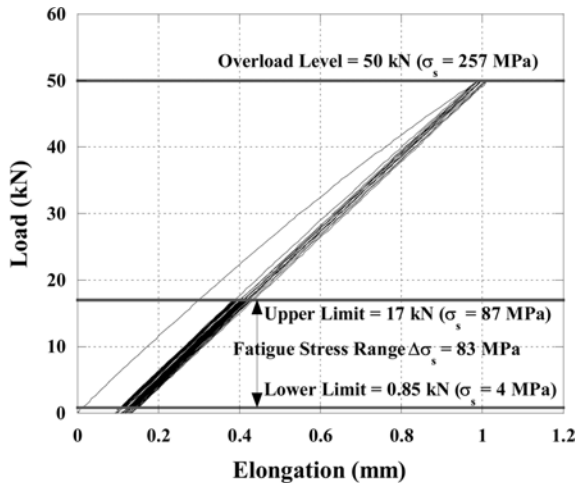

Fig. 10 Typical load-elongation response of the SDS configuration as a result of fatigue testing and intermittent overload

by corrosion, or structural elements originally designed to carry lower loads, it is envisaged that the assumptions made are not as redundant as they appear. Moreover, the adhesive bond may be required to transfer a portion of the dead load thereby causing the concurrent action of sustained and cyclic loading to raise the mean stress level. Hence the maximum fatigue stress level of 87 MPa, assumed herein, can become far less conservative than it may initially seem.

Despite the fact that the adhesive was loaded beyond elastic limits in the local areas around the ends of the composite strips, no visible damage was seen in the specimens as a result of fatigue loading. A typical trace of load-elongation is shown in Fig. 10. The initial hysteresis, associated with accumulation of permanent deformation, due to the concurrent effects of shear and peel stresses, was induced by the first 0-50-0 kN load/unload block. With increase in the number of fatigue cycles and in the presence of further intermittent overloads there was only a very small further increase in the permanent offset, although the bond itself still responded in linear elastic fashion without appreciable loss in stiffness. This behavior is consistent with the stated design philosophy of ensuring a sufficiently long lap-splice to avoid load-rate based plastic deformation effects.

Residual tensile strength after the 1 million fatigue cycles with periodic overloading was assessed by performing monotonic tensile tests on the specimens at the same rate of loading, 0.5 kN/s, used on the unfatigued specimens and results can be compared in Table 1. Failure was through debond initiation at the ends of the composite strips in a fashion similar to the non-fatigue specimens and at a similar level of load.

Debond initiation and separation of the strips was seen at approximately the same load and strain levels as seen in the un-fatigued specimens and as can be seen in a comparison of typical traces in Fig. 11 there is little difference in overall response between the two sets of specimens indicating that the fatigue loading had substantially no effect on overall response. It is of interest to note that all specimens carried loads in excess of those associated with yielding of the unbonded specimens prior to bond deterioration.

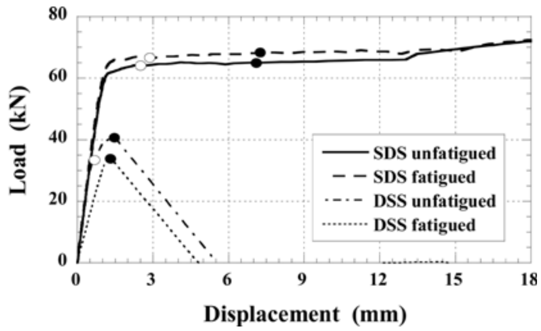

Fig. 11 Comparison of typical load-elongation traces of unfatigued and fatigued SDS and DSS specimens under monotonic tensile load. The unfilled and filled circles represent locations of disband initiation and patch separation, respectively.

Fatigue of the DSS configuration specimens was aimed at assessing response under a spectrum loading that repeatedly induced plastic shear strain in the adhesive. For this case the elastic limit tensile load can be calculated as

$$F_{e,DSS} = \frac{2\tau_p(1+S)w}{\lambda} = 8.8 \text{ kN} \tag{21}$$

The specimens were initially subjected to a 0-15-0 kN loading-unloading block, and then fatigued at a constant stress range of $\Delta\sigma_s$ = 73 MPa at R = 0.05 (with minimum and maximum loads of 0.75 kN and 15 kN, respectively) and at a frequency of 12 Hz for 1 million cycles. Changes in the response due to damage accumulation, resulting in increased crack opening displacement, were assessed by repeating the initial 0-15-0 kN load block every 250,000 cycles, and recording the applied load and

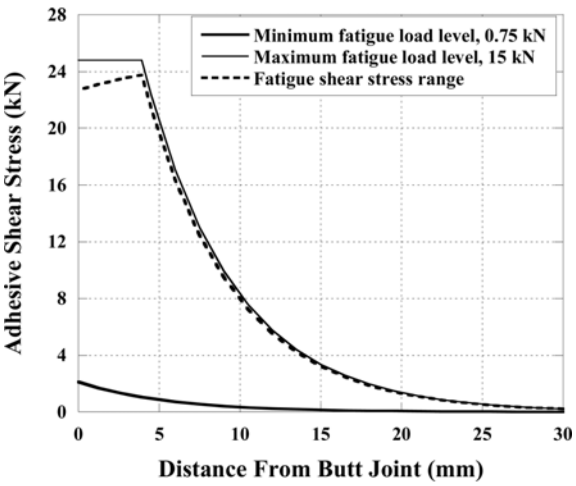

Fig. 12 Theoretical adhesive shear stress levels for fatigue in the DSS configuration as a function of distance from the butt-joint region

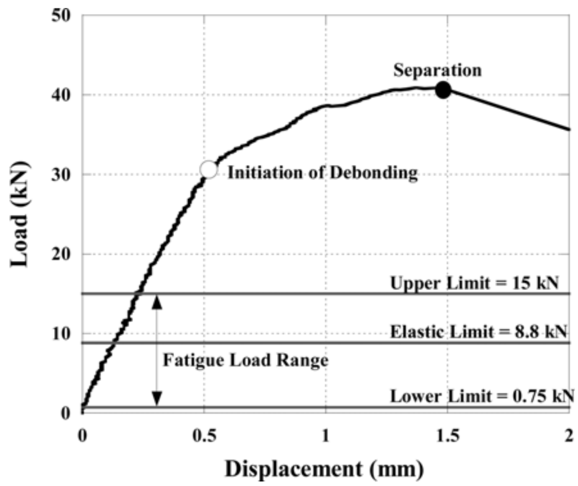

Fig. 13 Fatigue load levels in comparison to a typical DSS configuration response in tension

crosshead displacement during these blocks and after every 10,000 cycles. Due to a net joint stiffness imbalance, the maximum load resulted in the formation of shear stress plastic plateaus at the central location, where the steel bars butted together, while the normal stress was compressive and thus anti-peel. Fig. 12 shows the theoretical adhesive shear stress distribution in the vicinity of the central section at the pertinent load levels and the fatigue stress range along the bond line in the vicinity of the central section. A comparison of the fatigue load levels with the typical response of a double strap specimen (DSS) tested in monotonic tension is shown in Fig. 13.

In the DSS configuration partial debonding was seen, at the interface with both composite strips, initiating outwards from the central butt region with a growth rate between 6.5×10^{-8} m/cycle to 1.3×10^{-7} m/cycle. The maximum length of debond measured at the end of the cycling regime was about 63% of the overlap length on one side of the joint. A typical load-elongation plot is shown in Fig. 14, wherein the progressive increase in elongation with accompanied loss in stiffness can be essentially traced to effects of debonding of the composite strips. The effective disbond length was estimated from the displacement data by means of simple one-dimensional analysis. Since no crack initiated during the first load cycle, the differential elongation at F = 15 kN, $\Delta\delta_N$, between the initial load-unload block and that following the Nth cycle, can be related to the average crack length per lap splice, b_N, via the expression

$$\Delta\delta_N = \delta_N - \delta_1 \approx 2b_N\Delta\varepsilon_c = 2b_N(\varepsilon_{c,m} - \varepsilon_{c,l}) \tag{22}$$

wherein $\varepsilon_{c,m}$ and $\varepsilon_{c,l}$ are the CFRP strains, at F = 15 kN, in a bond section immediately outside the anchorage length (within the disbond-tolerant zone where no load is originally transferred, i.e., $\tau \approx 0$, indicated in Fig. 7(b)), and above the central butt-joint where the maximum tensile strain is attained, respectively. That is, the length of the damage-tolerant trough within each lap splice, $l - (L_{eff,0} + L_{eff,l})$, is expected to decrease by an average of b_N as the load cycling regime progresses. By assuming the theoretical $\varepsilon_{c,m}$ = 306 $\mu\varepsilon$ at x = 105 mm, where the average experimental ε_c from SG-1 (Fig. 5(b)) is 314 $\mu\varepsilon$, and $\varepsilon_{c,l}$ = 1,367 $\mu\varepsilon$ from equilibrium considerations, the average disbond length after the Nth fatigue cycle can be estimated rearranging Eq. (22) as

$$b_N \approx \Delta\delta_N/(2.122 \cdot 10^{-3}) \tag{23}$$

As reported in Table 2, the values computed at the end of the fatigue cycling, $b_{1,000,000}$, are in fair agreement with the average from visual inspection, obtained by summing the length of all visible crack fronts and then dividing by four. The increase in average disbond length values from (23)

Table 2 Comparison between calculated and observed crack lengths at N = 1,000,000 for three DSS specimens

Sample ID	$\Delta\delta_N$ (mm)	$b_{N,\text{analytical}}$ [Eq. (23)] (mm)	$b_{N,\text{observed}}$* (mm)	$b_{N,\text{analytical}}/b_{N,\text{observed}}$
DSS-1	0.233	110	117	0.93
DSS-2	0.193	91	80	1.14
DSS-3	0.203	96	90	1.07

*Average of all visible crack front lengths

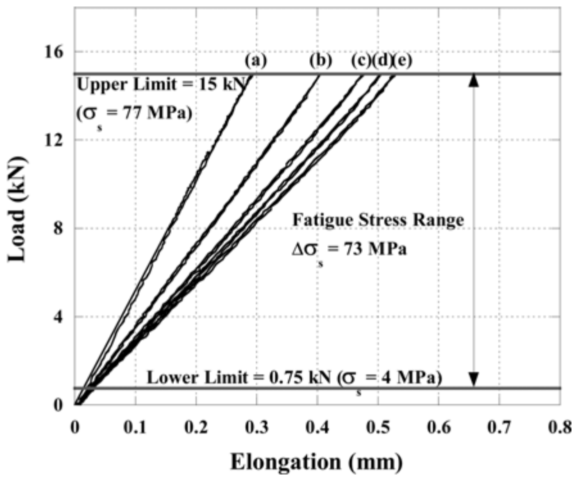

Fig. 14 Typical load-elongation response of the DSS configuration as a result of fatigue testing with intermittent overload (a) at 0 cycles, (b) at 250,000 cycles, (c) at 500,000 cycles, (d) at 750,000 cycles, and (e) at 1,000,000 cycles

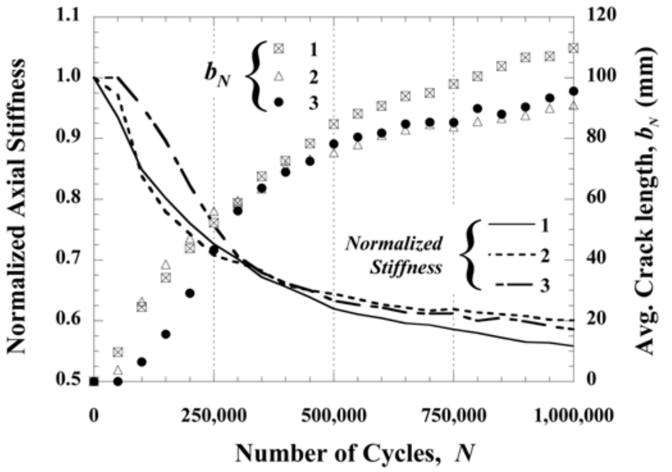

Fig. 15 Evolution of typical stiffness loss, and crack propagation, as a function of number of fatigue cycles for double strap specimens (DSS)

with increasing number of cycles for a set of DSS samples is shown in Fig. 15, along with the corresponding decrease in axial stiffness. The initial rapid crack growth is followed by a fairly linear trend from about 500,000 cycles, wherein the maximum crack growth rate $db/dN = 5.0 \times 10^{-8}$ m/cycle was determined by fitting a straight line to data. Upon completion of the fatigue test, a maximum fracture length of 130 mm was visually observed, i.e., 63% of the lap splice length, and 83% of the 157 mm damage-tolerant trough at F = 15 kN. The selected lap splice provided sufficient damage tolerance to enable effective load transfer during fatigue crack propagation, and after 1 million cycles the specimens were able to transfer the full load, albeit while retaining only 56-60% of the original stiffness

When loaded monotonically after completion of the fatigue loading the specimens failed in a

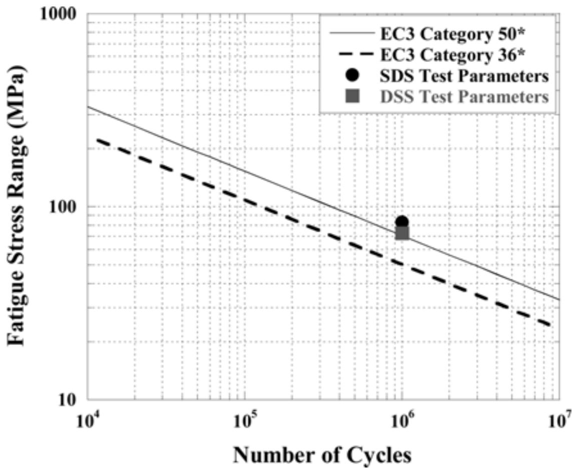

Fig. 16 Test parameters compared to EC3 category 36* and 50* response

brittle manner at an average load of 34.2 kN, retaining about 83% of the original load capacity with final failure occurring through a mix of cohesive failure within the adhesive and fiber-matrix debonding along planes in the composite strips themselves close to the bond line. In some cases the possibility of the influence of edge effects could be observed through arching in the disbond surfaces. It is pointed out that this more desirable failure mode did not replicate that observed in the SDS specimens, as the relatively small adhesive anti-peel stresses acting in the proximity of the butt-joint contributed to an essentially mode II fracture initiation, similarly to the unfatigued DSS specimens. Separation along the steel/adhesive interface in the SDS samples, and at the patch ends of some DSS samples once the low-stress trough was no longer available due to crack propagation, suggests that peeling effects played a major role in the failure mechanism. However, it is clear that the selected overlap length was sufficiently long to enable transfer even after partial debonding, thereby providing a level of damage tolerance.

5. Conclusions

Structural steel-composite skin doubler (SDS) and double strap (DSS) adhesively bonded specimens were tested both in monotonic tension and tensile fatigue regimes. As shown in Fig. 16 the stress ranges and number of cycles selected in the fatigue test regime are greater than the threshold levels required of performance for the EC3 categories 36* and 50* (European Committee for Standardization 1992) and AASHTO category E and E' details (Hart-Smith 2002), which include cover plates typically welded onto tension members for rehabilitation purposes. The SDS specimens were tested under constant amplitude fatigue, with periodic overloads of 84% of steel yielding. The bonds retained essentially the original stiffness and strength, and failed within the steel/adhesive interface due to peeling-off of the composite at a monotonic load 12% higher than that associated with yielding of the steel. Strain relief of 20% was also achieved in the metallic substrate, thus indicating the potential for rehabilitation of tension flanges of flexural members. The DSS samples were tested under constant amplitude fatigue, with a maximum load 70% greater than that associated with adhesive plastic transition in shear. Debonds propagated from the butt region as cycling progressed, resulting in a stiffness loss of 40-44%. The residual strength was 83-88% that of the unfatigued specimens, at a level where the maximum strain in the composite exceeded 20% of the ultimate. Failure was a combination of a cohesive mode in the adhesive and fiber-matrix debonding within the composite, whereas it was essentially cohesive in the unfatigued specimens. It is noted that the drop in performance could, in future, be avoided by adopting a more stiffness-balanced joint design. None-the-less, since the steel adherends had some oxide build-up on the surface after exposure to the atmosphere prior to bonding, the results emphasize the potential for use even in non-ideal pre-treatment conditions, together with the ability to build-in bond damage tolerance which is critical in applications wherein maintenance and inspection are likely to be infrequent.

Acknowledgements

The first author would like to acknowledge the support of the University of Padua and the University of California for enabling his research under the Education Abroad Program (EAP) scheme. The research was completed at the University of California San Diego. The generous support of DuPont in studying the rehabilitation of steel using FRP composites is gratefully acknowledged. The assistance of Sika in supplying the composite strips and the adhesive is also acknowledged.

References

Albat, A.M. and Romilly, D.P. (1999), "A direct linear-elastic analysis of double symmetric bonded joints and reinforcements", *Composites Science and Technology*, **59**(7), 1127-1137.

Albrecht, P. and Hall, T.T. (2003), "Atmospheric corrosion resistance of structural steels", *ASCE J. Mater. Civil Eng.*, **15**(1), 2-24.

Albrecht, P. and Sahli, A.H. (1988), "Static strength of bolted and adhesively bonded joints for steel structures", ASTM STP 981, Adhesively Bonded Joints: Testing, Analysis and Design. Ed. W.S. Johnson, 229-251.

American Association of State Highway and Transportation Officials (1998), "Load and resistance factor design (LRFD) bridge design specifications", 2nd edition.

Baker, A.A. and Jones, R. (1988), *Bonded Repairs of Aircraft Structures*, Martinus Nijhoff.

Bassetti, A., Nussbaumer, A. and Hirt, M.A. (2000), "Fatigue life extension of riveted bridge members using prestressed carbon fiber composites", *Proc. of the Int. Conf. on Steel Structures of the 2000's*, Istanbul, Turkey, September 11-13, 2000, 375-380.

Bourban, P.E., McKnight, S.H., Shulley, S.B., Karbhari, V.M. and Gillespie, J.W. Jr. (1994), "Durability of steel/composite bonds for rehabilitation of structural components", *Proc. of the 3rd ASCE Materials Engineering Conf.*, San Diego, CA, 295-302.

Colombi, P., Bassetti, A. and Nussbaumer, A. (2003), "Analysis of cracked steel members reinforced by pre-stress composite patch", *Fatigue and Fracture of Engineering Materials and Structures*, **26**(1), 59-66.

Dunker, K.F., Klaiber, F.W. and Sanders, W.W., Jr. (1987), "Bridge strengthening needs in the United States", *Transportation Research Record* 1118, Transportation Research Board, Washington, D.C., 1-8.

European Committee for Standardization (1992), "ENV 1993-1-1, Eurocode 3- Design of Steel Structures: Part 1-1: General Rules and Rules for Buildings".

Fisher, J.W. (1984), *Fatigue and Fracture in Steel Bridges: Case Studies*, John Wiley and Sons.

FRP Composites: Life Extension and Strengthening of Metallic Structures (2001), ed. by S.S.J. Moy, Institution of Civil Engineers Design and Practice Guide, Thomas Telford, London.

Grabovac, I. (2003), "Bonded composite solution to ship reinforcement", *Composites A*, **34**, 847-854.

Hart-Smith, L.J. (1973), "Adhesive-bonded double lap joints", NASA-CR-112235.

Hart-Smith, L.J. (2002), "Recent expansions in the capabilities of Rose's closed-form analyses for bonded crack patching", in Advances in the Bonded Composite Repair of Metallic Aircraft Structure, eds. A.A. Baker, L.R.F. Rose and R. Jones, Elsevier, 177-206.

Hollaway, L.C. and Cadei, J. (2002), "Progress in the technique of upgrading metallic structures with advanced polymer composites", *Progress in Structural Engineering and Materials*, **4**(2), 131-148.

Jones, S.C. and Civjan, S.A. (2003), "Application of fiber reinforced polymer overlays to extend to steel fatigue life", *J. Composites for Construction*, ASCE, **7**(4), 331-338.

Karbhari, V.M. and Shulley, S.B. (1995), "Use of composites for rehabilitation of steel structures – determination of bond durability," *J. Mater. Civil Eng.*, ASCE, **7**(4), 239-245.

McKnight, S.H., Bourban, P.E., Gillespie, J.W. Jr. and Karbhari, V.M. (1994), "Surface preparation of steel for adhesive bonding in rehabilitation applications", *Proc. of the 1994 ASCE Materials Engineering Conf.*, San Diego, CA, 1148-1155.

Moy, S.S.J. (2002), "Early age curing under cyclic loading – An investigation into stiffness development in carbon fibre reinforced steel beams," *Proc. of the Int. Conf. on Advanced Polymer Composites in Construction*, Southampton, UK, April 15-17, pp.8.

Moy, S.S.J., Barnes, F., Moriarty, J., Dier, A.F., Kenchington, A. and Iverson, B. (2000), "Structural upgrade and life extension of cast iron struts using carbon fiber reinforced composites", *Proc. of the 8th Int. Conf. on Fibre Reinforced Composites*, Newcastle upon Tyne, UK, September 13-15, 3-10.

Nara, H., Gasparini, D.A., Andreani, J. and Boggs, C. (1985), "Steel to steel bonding for bridges", *Proc. of the 30th Int. SAMPE Symposium and Exhibition*, Anaheim, CA. March 19-21, 1387-1396.

National Bridge Inventory (2002), "United States NBI Report 2002", http://www.nationalbridgeinventory.com/nbi_report_2002.htm

Nishikawa, K., Murakoshi, J. and Matsoukis, T. (1998), "Study on the fatigue strength of steel highway bridges in Japan", *Construction and Building Materials*, **12**(2-3), 133-141.

Poole, P. (2002), "Graphite/Epoxy patching efficiency studies", in Advances in the Bonded Composite Repair of Metallic Aircraft Structures, eds., A.A. Baker, L.R.F. Rose, and R. Jones, Elsevier, 415-441.

Sen, R. and Liby, L. (1994), "Repair of steel composite sections using CRFP laminates", Final report submitted to the Florida Department of Transportation, University of South Florida.

Shulley, S.B. (1994), "Application of composites to the rehabilitation of steel infrastructure", B.S. Thesis, University of Delaware, pp.60.

Shulley, S.B., Huang, X., Karbhari, V.M. and Gillespie, J.W. Jr. (1994) "Fundamental considerations of design and durability in composite rehabilitation schemes for steel girders with web distress", *Proc. of the 1994 ASCE Materials Engineering Conf.*, San Diego, CA, 1187-1194.

Tavakkolidazeh, M. and Saadatmanesh, H. (2003a), "Fatigue strength of steel girders strengthened with carbon fiber reinforced polymer patch", *J. Struct. Eng.*, ASCE, **129**(2), 186-196.

Tavakkolidazeh, M. and Saadatmanesh, H. (2003b), "Strengthening of steel-concrete composite girders using carbon fiber-reinforced polymer sheets", *J. Struct. Eng.*, ASCE, **129**(1), 30-40.

Tavakkolidazeh, M. and Saadatmanesh, H. (2003c), "Repair of damaged steel-concrete composite girders using carbon fiber-reinforced polymer sheets", *J. Composites for Construction,* ASCE, **7**(4), 311-322.

Wang, C.H. and Rose, L.R.F. (1997), "Determination of triaxial stresses in bonded joints", *Int. J. of Adhesion and Adhesives*, **17**(1), 17-25.